GPS Receiver Performance Using Inertial-Aided Carrier Tracking Loop

Tsung-Yu Chiou
Stanford University, Stanford, CA

BIOGRAPHY

Tsung-Yu Chiou is a Ph.D. candidate in the Aeronautics and Astronautics Department at Stanford University. He received his B.S. in Aerospace Engineering in 1998 from Tamkang University, Taiwan and his M.S. from Stanford in 2002. His research currently focuses on the performance analysis and validation of Inertial-aided GPS carrier-tracking loop.

ABSTRACT

Radio frequency interference (RFI) has been a perplexing problem, affecting the navigation quality of the Global Positioning System (GPS). The presence of the RFI, or even hostile jamming, will reduce the effective received signal power, and thus degrade navigation accuracy, continuity, and integrity of the system. A proposed next generation aircraft navigation system for the U.S. military called the Joint Precision Approach and Landing System (JPALS) [1, 2] is an example of a system that requires high performance even in severe RFI environments.

Previous research has proposed using inertial-aided GPS carrier-tracking loops as a component of the anti-jam solutions [3, 6]. It is believed that an inertial-aided GPS receiver is more robust to wide-band RFI. By eliminating the need to track platform dynamics, the inertially-aided GPS tracking loops can operate at narrow noise bandwidths, thus lowering the tracking thresholds to a lower carrier-to-noise (C/N0). As a result, the lower C/N0 thresholds increase robustness to the RFI.

The purpose of this paper is to verify the performance of an inertial-aided GPS receiver experimentally, since the performance has not been fully validated. A metric to evaluate the inertial-aided GPS receiver is, in wide-band RFI environments, the tolerable degradation of carrier-to-noise ratio (C/N0) and its corresponding loop bandwidth.

A unique and flexible inertial-aided GPS test-bed has been developed to conduct experiments to include various combinations of inertial measurement units (IMUs) with GPS receiver clocks. In addition to different choices of IMU, the GPS carrier-tracking loop can be implemented and modified using different orders of tracking-loop filters and various noise bandwidths. Moreover, the level of C/N0 is tunable by injecting various power levels of white Gaussian noise into the same collected GPS front end signals.

Future work will consider details of clock dynamics in inertial-aiding techniques. As shown in this study, the receiver clock phase error induced by the vibrating platform significantly limits the performance of the integrated GPS/INS navigation system. An accurate measurement of the power spectral density (PSD) of the receiver clock vibration and a precise estimate of the acceleration sensitivity vector are two building blocks for advancing this inertial-aiding technique. A better improvement of C/N0 is expected if a higher quality clock, such as an atomic clock, were used to drive the GPS receiver. In the low noise bandwidth range, the clock dynamics dominate the GPS receiver tracking performance.

I. INTRODUCTION

The Joint Precision Approach and Landing System (JPALS) [1, 2] is the next generation landing system for the U.S. military. JPALS will provide joint operational capability for U.S. forces to accomplish both conventional and special missions in a wide range of environments, which include not only various meteorological and terrain conditions, but also hostile radio-frequency interference (RFI) circumstances. Thus, integrity and continuity are the two most stringent requirements for JPALS. For example, the required integrity and continuity for the Sea-based JPALS, the Navy variant of the system, are 10^{-7} / approach and 2×10^{-6} / 15 sec., respectively[2].

However, the RFI poses a severe threat to GPS integrity and continuity. Therefore, mitigating RFI is a priority for the JPALS program. There are several techniques considered to reduce the effects of RFI on system integrity and continuity [3]. For instance a jamming-to-noise ratio (J/N) meter [4], receiver front-end filtering techniques, narrowband interference-processing techniques, or with antenna enhancement.

This paper focuses on yet another technique: code/carrier tracking loop aiding. This is accomplished by applying external aiding enhancements into code / carrier-tracking-loops. In this research, the external aiding source is an IMU.

In this integrated GPS/INS scheme [5, 6], the structure of the traditional GPS carrier-tracking loop is changed to enable the fusing of the externally estimated Doppler frequency, provided by inertial measurement units, into the carrier-tracking loop. This inertially-aided tracking loop allows the reduction of the carrier-tracking loop bandwidth, by eliminating the need to track the platform dynamics. The extra Doppler frequency shift caused by the motion of the GPS receiver defines the platform dynamics. The above frequency shift usually changes rapidly with time, and therefore increases the burden of the carrier-tracking loop to lock in the phase. With an inertially-aided tracking loop, the IMU defines the extra dynamics, so that the tracking loop does not have to track these rapid frequency shifts. A lower noise bandwidth is sufficient, making the receiver more able to reject noise. As a result, it is more robust to the wide-band RFI. Previous research in [7] has shown that an additional 4 to 5 dB-Hz margin on carrier-to-noise ratio (C/N0) can be achieved using the inertial-aiding technique.

Based on previous studies, an experimental validation is implemented in this study to test the GPS performance in a wide-band RFI environment. A flexible test-bed has been developed to validate the inertial-aiding technique. Using this test-bed, we can test the performance of carrier-phase measurements for combinations of different orders of carrier-tracking loops, different coherence integration times, different receiver oscillators, and different inertial measurement units, and all under varying wide-band interference. Specifically, this paper provides results focusing on the performance for different orders (second and third-order loops) of carrier-tracking loops, combined with two types of GPS receiver oscillators. Furthermore, the results are evaluated based on various noise bandwidths and different C/N0 conditions. The tunable bandwidth is accomplished using a software receiver and the adjustable C/N0 is achieved by injecting white Gaussian noise into the sampled GPS front-end signals

II. OVERVIEW OF GPS CARRIER-TRACKING LOOPS

To understand the inertially aided carrier-tracking loop and the results of this paper, understanding how the GPS carrier-tracking loop functions is essential. This section presents an overview of GPS carrier-tracking loops. More thorough discussions of the GPS carrier-tracking loop are provided in [3, 8 and 9]. A GPS L1 signal consists of the navigation data, the Coarse/Acquisition (C/A) code, and the Radio-Frequency (RF) carrier. The GPS antenna captures the GPS signals in view; the signals then pass through the RF front end and are sampled as well as down-converted to a proper intermediate frequency (IF) (1-20MHz). At this point, the GPS signal superimposes all the signals from the satellites. Numerous parallel channels are required to acquire and track the signal from each satellite. At each channel, upon acquiring a signal from a satellite, a phase-locked loop is used to track the phase and frequency of the carrier. Figure 1 shows the structure of a generic GPS phase-locked loop [3], with or without Doppler-aiding input.
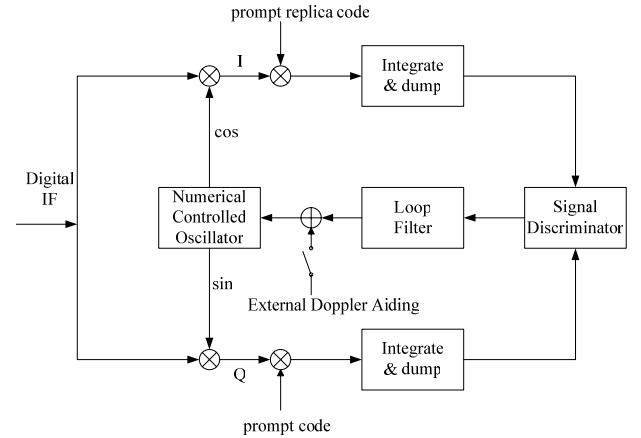

Figure 1: GPS carrier-phase tracking loop

To extract the navigation data, the digital IF input must be further down-converted to the baseband. This is called a carrier wipeoff operation which is performed by multiplying the carrier replica, as shown by the first pair of multiplication in Figure 1. The frequency of the replica carrier used for this down-conversion is obtained by measuring the frequency and phase offset due to platform motion and clock dynamics. As a result, this is the heart of the PLL. The device generating the replica carrier is usually a voltage-controlled oscillator (VCO) or mathematically represented by a numerically-controlled oscillator (NCO). The upper branch multiplied by the cosine carrier replica is called the in-phase channel (I), while the lower branch multiplied by the sine carrier replica is called the quadrature channel (Q). I and Q

signals here are primarily the result of the multiplication of the thermal noise and the replica digital cosine and sine wave, respectively. In other words, the desired signal is still buried under the thermal noise floor. To collapse the I and Q signals to the baseband, a code-stripping process is required. This code wipeoff process is achieved by multiplying the I and Q channels by the prompt code replica.

Thereafter, the signal has been down-converted to the baseband, and the predetection integration process is executed in an "integrate and dump" operation, which performs measurement-averaging over at least one or more code periods. The longer the averaging time is, the more noise is suppressed. The output of this process is the input to a phase discriminator, which measures the phase offset between the true carrier and the replicated in-phase carrier. One example of the phase discriminator is the arctangent of Q/I. The output of the phase discriminator is the phase angle of the vector sum of I+Q with respect to the I-axis. This phase angle is then used as a control command to the loop filter. The loop filter is a compensator designed to track the phase (and frequency) of the input carrier with the desired dynamic range and noise suppression performance. The output of the loop filter is a frequency command for the NCO, which steers the replicated carrier frequency to lock in the phase. As a result, the objective of the carrier-tracking loop or phase-locked loop (PLL) is to maintain the phase error between the replica carrier and the input GPS carrier signals at zero. Therefore, the phase error is an important parameter to characterize the performance of the PLL.

To analyze the phase error of the PLL, a linear model illustrated in Figure 2 is usually used. The input φ_i is the phase of the incoming digital IF signal. The output φ_o is the phase steered by the PLL to track the input φ_i. The summation symbol in Figure 2 represents the phase discriminator in Figure 1. Thus, $\delta\varphi$ is the phase error between φ_i and φ_o. Ideally, $\delta\varphi$ stays exactly at zero once the phase is locked in. However, the incoming phase signal φ_i is influenced by the thermal noise, the dynamics of the platform, and even the satellite clock dynamics. Furthermore, the replica carrier phase φ_o is affected by the receiver clock dynamics and an extra phase instability induced by the platform vibration. As a result, the phase error source includes the thermal noise, platform dynamics stress error, receiver and satellite clock dynamics, and the receiver clock error induced by the platform vibration.

A higher bandwidth PLL has better performance on tracking the dynamics. However, a higher bandwidth PLL demonstrates poor quality on noise suppression.

Therefore, a trade-off is needed when designing a PLL. The phase error response is a parameter for judging the proper PLL bandwidth. The standard deviation value (1-sigma) of the steady state phase error is of interest in this paper. 1-sigma phase error is used as a metric to characterize the performance of the PLL alone or the inertially-aided PLL. Note that the PLL phase error is the phase difference between the local replica and the incoming signal. The 1-sigma phase error can be represented as equation (A13).
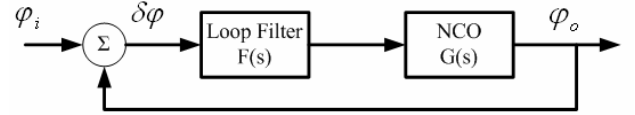

Figure 2: A Liner Model of a Phase-Locked Loop

III. INERTIALLY AIDING CARRIER-TRACKING LOOP

Following the above discussions of PLL phase error, one can consider removing the dynamic stress error by applying inertial aiding. Note that the inertial aiding contributes to the PLL by providing the estimated Doppler frequency due to any motion between the receiver and the satellite. Figure 3 shows a linear model of the PLL with Doppler aiding. f_{PLL} represents the carrier-frequency deviation from the intermediate frequency (IF). As discussed in the previous section, this frequency deviation is primarily comprised of three components: the Doppler frequency (f_{dopp}) due to the relative motion between the receiver and the satellite; frequency errors due to receiver or satellite oscillators (f_{clk}); and errors due to thermal noise and interference (f_{noise}). Equation (1) represents f_{PLL} in terms of these components.

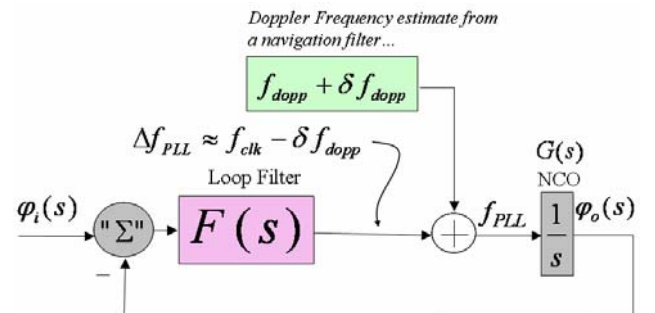$$f_{PLL} = f_{dopp} + f_{clk} + f_{noise}. \tag{1}$$

Figure 3: A Liner Model of a Phase-Locked Loop with Doppler-aiding

Inertial aiding is implemented by adding the external Doppler-frequency estimate to the output of the loop filter. This external input may be calculated from a GPS/INS navigation filter, whose navigation outputs are primarily based on inertial measurements in the short term. Inclusion of the external Doppler-frequency estimate removes the task of tracking vehicle dynamics from the PLL, but may introduce a different form of dynamic stress in the form of errors from the external Doppler estimates. Therefore, the PLL with Doppler-aiding must be designed to track phase-dynamics due to the receiver oscillator instability and Doppler-estimate errors. As a result, the value of the loop-filter frequency output for an inertial-aided PLL is

$$ f_{PLL} \cong f_{clk} + f_{noise} - \delta f_{dopp} . \tag{2} $$

Assuming that the dynamics of the Doppler-estimate errors are slower than vehicle dynamics, the use of Doppler-aiding allows for noise bandwidth reduction when compared to a traditional PLL, hence, improving its noise-suppression performance.

The focus of this paper is to provide the experimental results of the inertial-aiding technique, using the test-bed developed by the GPS lab at Stanford University. In the section highlighting test results, the performance of 1-sigma phase error as a function of PLL closed-loop noise bandwidth as well as C/N0 is evaluated.

IV. DATA COLLECTION AND EXPERIMENTAL SETUP

Data Collection Experiment

The data collection experiment was conducted with an automobile driven on a top level of a three-story parking structure. To include both static and dynamic data, the following drive-test scenario was used: the vehicle was static for 4 minutes, and then drove one loop around the top level of the parking structure (about one minute of movement). Figure 4 illustrates the profile of the horizontal speed in km/hour. The same data collection scheme was repeated with two different GPS reference oscillators: an oven-controlled crystal oscillator (OCXO), and a temperature compensated crystal oscillator (TCXO). In addition to the GPS data, an automotive grade IMU was included to provide the external Doppler estimate, such that the phase error performance could be studied for different combinations of GPS clock with the IMU. A set of three antennas in an equilateral triangle configuration was used as part of an automobile GPS attitude system, to measure the vehicle attitude as part of the measurement vector for the navigation filter[13]. The IMU and GPS antennas are

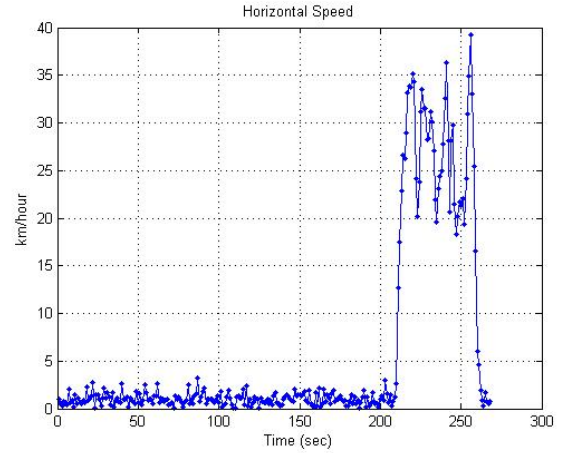shown in Figure 5, mounted on a rigid frame fixed on the test-vehicle's roof rack.

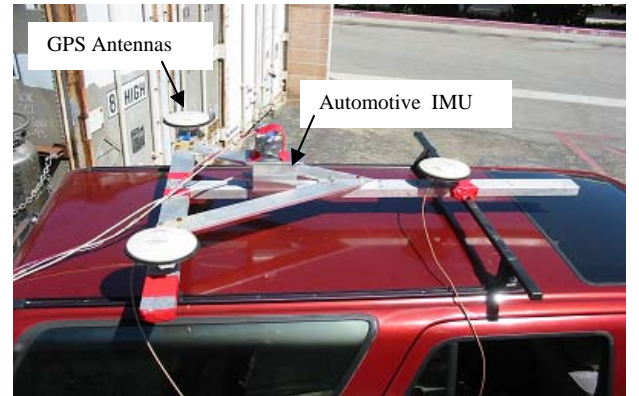**Figure 4: The Horizontal Speed of the Collected Data**

Figure 5: The Triangular Antenna Array and the IMU

The antenna array shown has 1 meter baselines; the IMU is mounted near the geometric center of the antenna array to simplify the kinematic equations of the navigation filter. Three Novatel Allstar GPS receivers are connected to the three antennas, and to a common clock to allow attitude determination with single-difference carrier-phase measurements.

Data Collection Hardware Setup

Figure 6 depicts the data collection hardware setup. The front end of a NordNav software receiver down-converts the L1 GPS signal to a 4.1304 MHz IF; the streamer samples the data at 16.3676 MHz.

As shown, one of two GPS reference oscillators could be used, and two sets of GPS front-end data were collected, one for each type of reference oscillator. The second branch of the data-collection setup includes three

Novatel receivers and an automotive grade IMU. A GPS/INS attitude system was utilized to provide attitude measurements at 10 Hz, in addition to the 10Hz velocity and 2Hz position measurements provided by the GPS receivers. In addition, the attitude system includes circuitry to generate a 100Hz-sampling signal, synchronized to the pulse-per-second signal from one of the Novatel receivers, which allows for the GPS time-tagging of IMU measurements. Table 1 summarizes the key components used for this experiment.
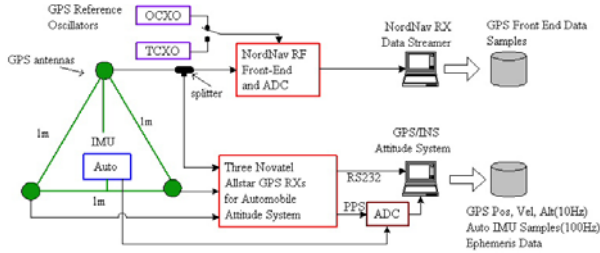
Figure 6: The Data Collection Hardware Setup

Table 1: Key Experiment Hardware

Equipment	Function
GPS	
1 NordNav R30 Receiver	✧ Provides the degree of freedom to modify the tracking loops, such that the estimated Doppler can be adopted. ✧ Collects, down-converts and samples the GPS data by the front end, so that the collected GPS data can be post-processed repeatedly using different tracking-loop filter orders/noise bandwidths, different C/N0, and different combinations of receiver clock with the IMU.
3 Novatel Allstar Receivers	✧ Form the triangular antenna array providing the initial calibration to the IMU. ✧ Provide the pulse per second information to a navigation filter, so that the GPS and IMU data can be synchronized.
1 TCXO	✧ Drives the NordNav R30 Rx.
1 OCXO	✧ Drives the NordNav R30 Rx.
IMU	
1 Automotive grade IMU	✧ Provides the position, velocity, and attitude to calculate the estimated Doppler frequency for the NordNav receiver.

Others		
Antenna Array	✧	Provides a rigid framework to calculate the initial attitude.
2 Laptop PCs	✧	Run the required programs and store the data.

V. POST PROCESSING PROCEDURE

The post-processing procedure consisted of two steps. First, the recorded GPS measurements from the Allstar receivers (position, velocity, attitude) and synchronized IMU data were passed through a GPS/INS navigation filter; the filter's velocity estimates were used along with satellite ephemeris data to compute Doppler estimates. Second, the Doppler estimates were used to implement inertially-aided phase-tracking on the recorded GPS IF samples. This step was accomplished using a modified NordNav software receiver, customized to process external Doppler information in replay mode. Figure 7 illustrates the post-processing procedure. As shown, the two key components are the GPS/INS navigation filter and the modified NordNav software receiver. The details of the navigation filter are beyond the scope of this paper, but it is important to note that the dynamic equations are written for the overall car position and velocity, including its suspension dynamics. In addition, the navigation filter velocity estimates always represent a blended GPS/INS solution; as a result no GPS outages have been included in the data at this time. It will be shown that the IMU sensor instability is negligible in the accuracy of Doppler estimates while GPS calibration is available at a high rate (10Hz in this case), but sensor instability is expected to have a significant impact on dead-reckoning mode when the GPS navigation solution is not present.

Finally, data pass through the other key component-the modified software receiver. The carrier-tracking loops are modified such that the estimated Doppler frequency from the GPS/INS navigation is fused into the phase-lock loop of the software receiver. The estimated Doppler is added directly to the original command output from the loop filter. After a transition period, the Doppler term in the original command output from the loop filter drops down to zero, as the dynamics have been removed by the externally estimated Doppler. One should note that this aiding scheme is equivalent to applying a frequency step into the PLL, unless the integrator outputs in the loop filter are reset when Doppler-aiding is applied. An initial frequency step that is too large would cause the loss of lock, since the frequency step may exceed the pull-in range of the PLL. Therefore, one possible scheme for the transition into an inertially-aided mode is to increase the frequency-aiding

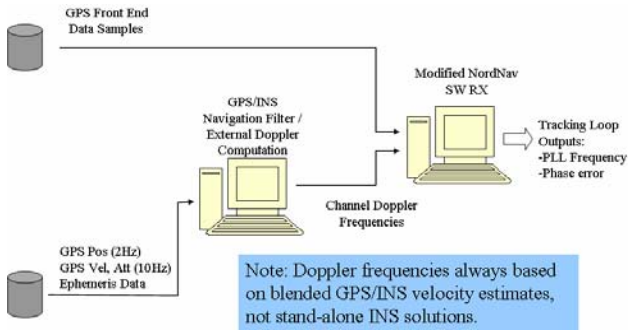gradually, so that the PLL can track the smaller rate of change in input frequency.

Figure 7: Post Processing Procedure

VI. RESULTS AND DISCUSSIONS

Estimated Doppler Frequency

As discussed previously, the PLL phase error performance depends on its bandwidth, signal-to-noise ratio, the quality of GPS reference oscillator, and in the case of an inertial-aided PLL, the accuracy of external Doppler estimates. Before showing the phase error performance with a different combination of GPS clocks and the IMU, it is instructive to illustrate the quality of receiver clocks and the quality of the estimated Doppler from the blended GPS/INS navigation filter. Figures 8 and 9 show the channel frequencies using the two different clocks and the corresponding estimated Doppler frequencies, computed with velocity outputs from the GPS/INS navigation filter (using the automotive IMU). The channel frequencies on each plot reflect the scenario of the test drive: for the first 3-4 minutes, the vehicle was stationary and began to move only at the beginning of the last minute. The blue line in Figures 8 and 9 serves as a reference for the estimated Doppler from the GPS/INS navigation filter. This line is the estimated Doppler frequency, calculated using the surveyed starting point of the tests and the satellite positions. Obviously, this estimate is valid only when the receiver is static. As can be seen in Figures 8 and 9, the estimated Doppler frequency captures the dynamics detected by the GPS receiver. The residual errors are those due to GPS clock dynamics, vibration induced errors, and thermal noise. Note that these remaining error sources are not included in the estimated Doppler to aid the traditional PLL. As can be seen in Figure 9, the Doppler frequency calculated by the GPS receiver (the red line) with OCXO is excessively unstable. This phenomenon is unexpected, but it causes a significant degradation in the phase error performance, as will be seen in the later plots.
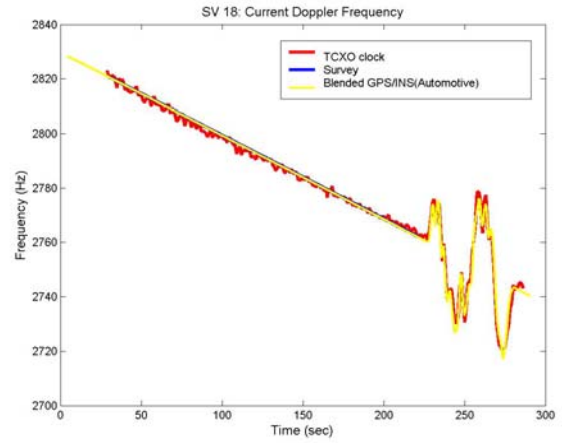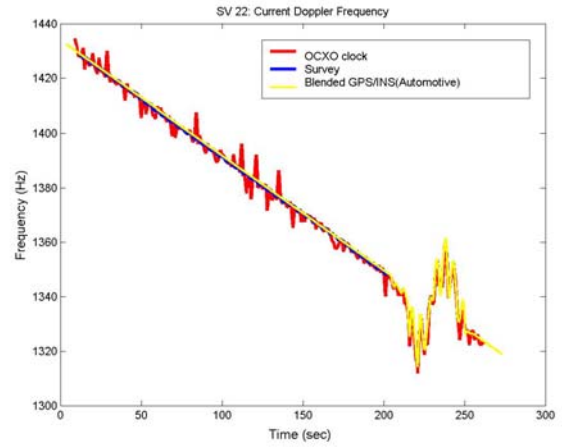

Figure 8: Channel Frequencies with TCXO

Figure 9: Channel Frequencies with OCXO

1-Sigma Phase Error versus PLL Noise Bandwidth

It is important to note that the following 1-sigma phase error shown on the plots is measured during the dynamic period. The improvement of the PLL when the GPS receiver is in motion is more important than the improvement when the receiver is static. Thus, the 1-sigma phase error here represents the steady state 1-sigma phase error when the receiver platform is in motion. Moreover, in Figures 10, 11, 12 and 13, the left end of each line of the experimental results indicates the lowest tolerable noise bandwidth in this investigation. This criterion is selected in order to find the lowest threshold of the test-bed. At the PLL design point, a 1-sigma phase error criterion (15 degrees for example [3]), would be used to determine the performance of the PLL.

Note that, for all the data shown in this paper, the coherent integration time (Tcoh) of the GPS tracking loops is 1 msec. Having a longer Tcoh, the GPS tracking loops average out more noise, as a result, can tolerate

lower C/N0 thresholds. 1 msec. is chosen as a baseline for this paper; investigating the dynamic tracking performance and validating the model is an essential starting point for examining the inertial-aiding technique.

One may be curious about the difference in performance between a second-order PLL and a third-PLL, with or without inertial aiding. Therefore, both orders of PLL have been implemented in the modified PLL of the software receiver. Figures 10, 11, 12 and 13 show the experimental results as well as the model results of the phase error performance in terms of various noise bandwidths.

The most important information in Figures 10, 11, 12, and 13 is the bandwidth reduction contributed by the inertial-aiding technique. For example, in the second-order PLL in Figures 10 and 11, the lower tolerable noise bandwidth is reduced from 7 Hz (unaided PLL) to 3.5 Hz (aided PLL). Note that the above values are read from the left stop points of the both blue curves. If the 15 degrees threshold is used as a metric, for example, the bandwidth reduction using the second-order PLL is 2.7 Hz. It should be noted that the relative bandwidth reduction depends on the receiver motion. In addition to examining the bandwidth reduction, it is more important to explore the allowable noise bandwidth when the PLL is aided, given the C/N0 and coherent integration time.

When the noise bandwidth is high (>=20Hz), it is expected, for both clocks, that there will be no difference in either second and third-order or unaided and aided PLL. In the high bandwidth region, the thermal noise is dominant. Thus, changing the loop order or applying inertial aiding does not improve the performance at all.

Another highlight point in Figures 10, 11, 12 and 13 is the fact that the second-order PLL has a larger bandwidth reduction given the same phase error, or a larger phase error reduction, given the same bandwidth than those of the third-order PLL. The reason for these phenomena is that as expected, the third-order PLL has a better dynamic tracking performance without inertial aiding than the second-order PLL. Consequently, the foregoing leads to an interesting result, which is the almost equal improvement gained from inertial aiding compared to the second-order PLL and the third-order PLL. This fact can be seen from the circle marked red and blue squared curves in Figure 11. A theoretical model [7], the solid green and dashed blue curves in Figure 11, also indicates this fact. The Appendix gives the details of the derivations for the 1-sigma phase error model of a PLL.
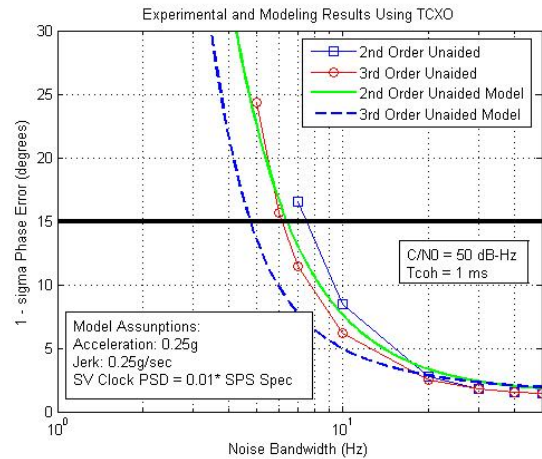

Figure 10: PLL Performance Driven by the TCXO with respect to the Noise Bandwidth and Comparison with Model Results for the case of Unaided PLL
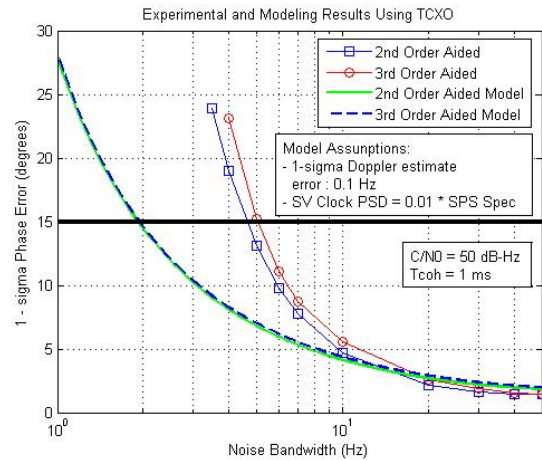

Figure 11: PLL Performance Driven by the TCXO with respect to the Noise Bandwidth and Comparison with Model Results for the case of Aided PLL
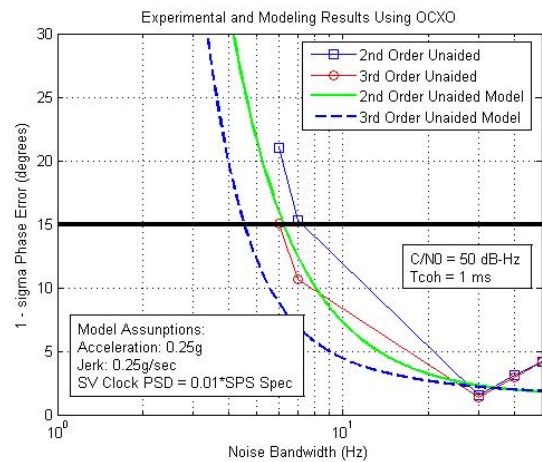

Figure 12: PLL Performance Driven by the OCXO with respect to the Noise Bandwidth and Comparison with Model Results for the case of Unaided PLL
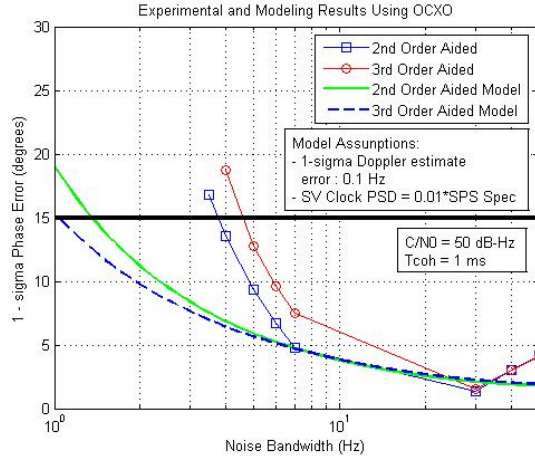
Figure 13: PLL Performance Driven by the OCXO with respect to the Noise Bandwidth and Comparison with Model Results for the case of Aided PLL

The reason that the aided third-order PLL is not always superior to the aided second-order is interesting. The foregoing point highly depends on the transient response of the PLL to the imperfect estimated Doppler frequency from the navigation filter and to the GPS clock dynamics. To highlight the response change related to the inertial aiding, I would like to discuss the impact of imperfect aiding. Without losing generality, we can model the aiding error by a 0.1 Hz frequency step input to the PLL [7]. From Equations (A29) and (A30) in the Appendix, the residual phase error due to the imperfect Doppler frequency estimate is given by the following Equations (3) and (4) for second-order and third-order PLLs, respectively.

$$\theta_{e2nd} = 86 \frac{\Delta f}{BW} \quad in \ \deg rees \ . \qquad (3)$$

$$\theta_{e3rd} = 90 \frac{\Delta f}{BW} \quad in \ \deg rees \ , \qquad (4)$$

where Δf the frequency step in Hz; BW is the noise bandwidth (Hz) of the tracking loop. Figure 14 shows the plots of Equations (3) and (4) and indicates the minimal difference between the two orders of the aided PLLs when a TCXO is used. This phenomenon can be seen from experimental results in both cases of oscillators. However, the model shown in Figure 13 indicates a contradiction way. The reason is that the clock dynamics given by equations (A20) and (A21) behave different between TCXO and OCXO. For the case of OCXO, the different responses of the two PLLs to clock dynamics overcome the difference shown between equations (3) and (4). As will be seen in the later sections, the clock model has to be further investigated. In short, equations (3) and (4) as well as the experimental results suggest that the

third-order aided PLL is not necessary outperform the second-order aided PLL.

Due to the excessive instability of the OCXO as shown in Figure 9, it is more constructive to look at results using TCXO. The experimental results and the model, shown in Figures 10 and 11, match to each other relatively well at the high operating noise bandwidth range (> 20 Hz). It is clear that the thermal noise error dominates the phase error at high bandwidth regime and the model also predicts analogous phase error. However, the model is too optimistic at the low bandwidth region. The discrepancy between the model and the experimental results in the low bandwidth region is due to the vibration model. The vibration PSD, as shown in Figure A1, used for the model is obtained from an aircraft dynamics. This PSD may not be identical to the car dynamics especially in low frequency part. Another dependent factor is the g-sensitivity of the oscillator. It is assumed to be 10^-9 parts/g across the whole spectrum of the vibration PSD. The actual condition of the oscillator, however, is changing with time, temperature etc. Therefore, it is critical to have a higher fidelity of the vibration PSD for a car movement and an accurate knowledge of the oscillator g-sensitivity.
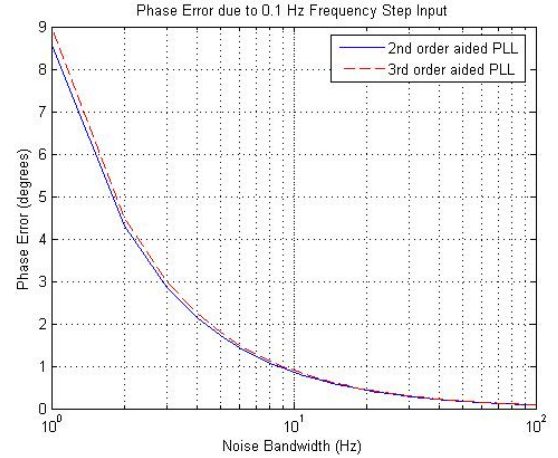

Figure 14: Residual Phase Error due to Imperfect Inertial Aiding (Model Results Using TCXO)

1-Sigma Phase Error versus C/N0

The other metric used to evaluate the effectiveness of inertial aiding is the allowable reduction of C/N0 that maintains the phase lock under dynamic conditions.

As indicated, Figures 15 and 16 show the 1-sigma phase error with respect to various C/N0 values. Note that the noise bandwidth for both plots is 7 Hz and the coherent integration time is 1 ms. Obviously, given the same C/N0, the phase error has been reduced by

applying the inertial aiding. The improvement in inertial aiding is minimal when the GPS receiver operates at a relatively high bandwidth. At low bandwidths, the dynamic stress dominates the phase error. Therefore, inertial aiding benefits are apparently in the low noise bandwidth range.

The 1-sigma phase error does not change with C/N0 when the C/N0 is above 40 dB-Hz. It is as expected since the phase error is dominated by the dynamics when the noise bandwidth is fixed at 7 Hz. As the C/N0 becomes lower, the thermal noise error starts to dominate the total phase error. The model results are also shown in green-solid and blue-dashed curves for aided second order PLL and third order PLL, respectively. Therefore, in Figures 15 and 16, the blue-circled and red-circled curves should line up with the green-solid and blue-dashed curves, respectively. As can be seen in Figures 15 and 16, the discrepancy between the model and the experimental results is relatively flat when the C/N0 is high. This constant offset indicates that the clock model and the vibration PSD used for the study do not truly represent the condition of this experiment. However, this discrepancy decreases as the C/N0 decreases since the thermal noise dominates the total phase error. Comparing this phenomenon with the high bandwidth region shown in Figures 10 and 11, we have a higher fidelity for the thermal noise model.
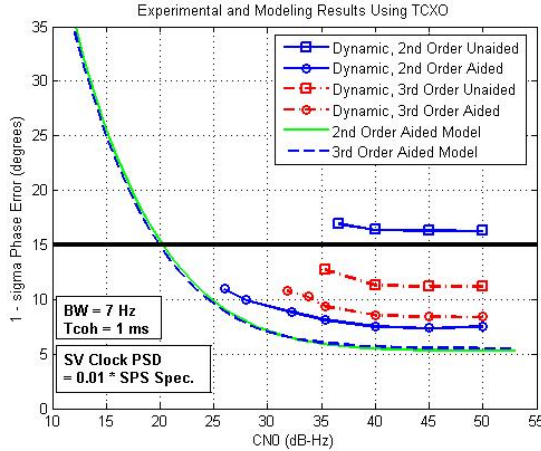

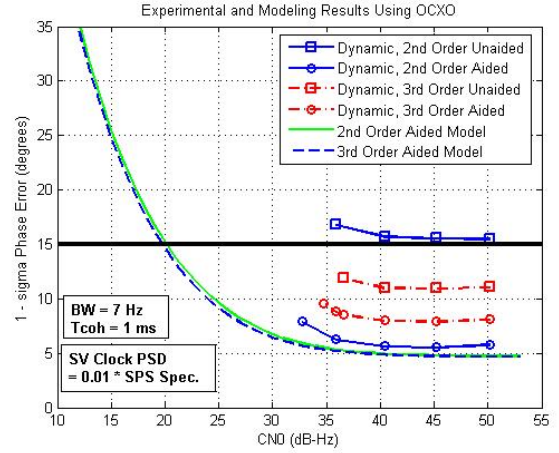**Figure 15: PLL Performance Driven by the TCXO with respect to C/N0; BW = 7Hz**

Figure 16: PLL Performance Driven by the OCXO with respect to C/N0; BW = 7Hz

VII. CONCLUSIONS

The technique of inertially aiding GPS tracking loops has been shown to effectively mitigate the RFI. This improvement is accomplished by applying the externally estimated Doppler frequency to the GPS carrier-tracking loop, so that the bandwidth required to track high dynamics is eliminated. Therefore, a lower noise bandwidth can be maintained in a high dynamic environment as well as when the RFI is present.

The experimental results show that we indeed have the improvement in the RFI, achieved by an inertial aiding technique. However, the amount of the RFI improvement is constrained by various factors such as receiver clock quality, the residual error of the inertial aiding, and even the stability of the power supply to the experimental set-up. One would expect a better result if an atomic clock were used. Therefore, the results of this paper provide a baseline model verification of the inertial-aided tracking loops.

The other interesting point is that the second-order loop performs better than the third-order loop when inertial aiding is applied. The reason is illustrated in Equations (3), (4), and Figure 14; the peak phase error of the second and third-order PLLs due to the residual error of the external frequency estimate is nearly equal. The foregoing is based on the assumption that the residual of the Doppler estimate is a frequency step. Indeed, the experimental results show that the assumption is reasonable.

The impact of receiver clock quality on the GPS/INS integrated system is shown in Figure 17, which illustrates the extra phase error induced by acceleration (or vibration). The two curves in Figure 17 indicate the extra induced phase error caused by platform acceleration.

These are experimental results found as the difference between the 1-sigma phase error before and after car motion. Since the induced clock phase error must be tracked by the PLL but not rejected, it is therefore a function of the noise bandwidth of the carrier tracking loop. From Figure 17, we notice that the induced phase error restricts the amount of PLL bandwidth reduction, which is the benefit of using the inertial-aiding carrier tracking loop. When the noise bandwidth is reduced below 10 Hz, the phase error is dominated by the clock dynamics. Even were the Doppler frequency introduced by the platform motion perfectly removed, the phase error due to clock dynamics eats up the margin originally preserved for the thermal noise phase error. Therefore, it is essential to understand the clock sensitivity to the acceleration and vibration modes of the receiver platforms. Given this understanding, the integrity requirements can be met by suitable adjustment of the phase error bound.
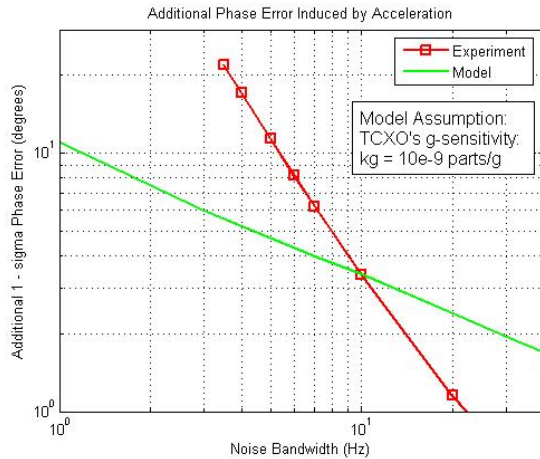

Figure 17: Additional 1-sigma phase error induced by receiver clock acceleration (TCXO)

The other information we can read from Figure 17 is the discrepancy between the model and the experimental result. This is due to the PSD used for the model is from an aircraft environment, which is not equivalent to the car movement. As mentioned, the g-sensitivity of the oscillator is also an important factor needed to be considered. Each oscillator has different reactions to vibration and acceleration.

In conclusion, a test-bed for the inertial aided carrier tracking loop has been fully implemented. The performance of this aiding technique is limited by the clock dynamics. To predict the performance by the model, a further validation on the model has to be conducted. The discrepancy between the model and the experimental results has been identified, which is the clock dynamics including clock phase noise as well as the clock sensitivity to vibration and acceleration.

VIII. FUTURE WORK

As observed in this paper, the GPS receiver clock plays an important role in the tracking loop enhancement technique. To study the clock dynamics, an elaborate experiment is needed. Applying acceleration on different cut sections of a crystal oscillator will excite different modes of clock noise and the vibration-induced errors. Thus, conducting an experiment on a shake table would be a subtle way to investigate the clock dynamics. Furthermore, a shake table can duplicate the vibration modes collected from real environments. Especially for JPALS applications, various vibration dynamics on an aircraft can be duplicated on a shake table.

IX. ACKNOWLEDGMENTS

APPENDIX

The performance of the carrier-tracking loop depends on the system order, system type, and the system noise bandwidth. The loop filter is designed to reduce noise, as well as to handle the signal dynamics. In this study, a first order and a second-order filter are implemented in the software receiver. Since the NCO is an integrator, the overall system is second-order and third-order, respectively. The following paragraphs provide the transfer functions and system characteristics of these two different orders of PLL.

Second-order Loop

For a second-order PLL, a proportional integral (PI) low-pass filter is considered first. The transfer function of the PI filter is given as follows:

$$F(s) = \frac{1 + \tau_2 s}{\tau_1 s}. \tag{A1}$$

Since F(s) includes a pole at s=0, the system shown in Figure 2 is a Type II system. This means that the steady-state error of the closed loop system is zero with a phase ramp input, which is equivalent to a frequency step input. The resulting closed-loop transfer function with this PI filter is

$$H(s) = \frac{\varphi_o}{\varphi_i} = \frac{G(s)F(s)}{1 + G(s)F(s)} = \frac{2\xi\omega_n s + \omega_n^2}{s^2 + 2\xi\omega_n s + \omega_n^2}, \tag{A2}$$

where $\omega_n = \sqrt{\dfrac{1}{\tau_1}}, and \quad \xi = \dfrac{\omega_n \tau_2}{2}$. ω_n is called the natural frequency of the second-order loop; ξ is called the damping ratio. An important characteristic of the PLL is its single-sided, closed-loop noise bandwidth (BW), which is defined as follows [10]:

$$BW = \int_0^\infty |H(j2\pi f)|^2 df. \tag{A3}$$

Evaluating Equation (A3) for this second-order loop PLL, gives the relationship between BW and ω_n as [10]:

$$BW = \frac{\omega_n}{2}(\xi + \frac{1}{4\xi}), \tag{A4}$$

where the units of BW and ω_n are Hz and rad/sec, respectively. For further analysis of the phase error in later sections, calculating the phase error to input transfer function ($H_e(s)$) is needed. Equation (A5) gives the definition and the specific expression of $H_e(s)$.

$$H_e(s) = \frac{\delta\varphi}{\varphi_i} = 1 - H(s) = \frac{s^2}{s^2 + 2\xi\omega_n s + \omega_n^2}. \tag{A5}$$

Of interest is the term $|H_e(s)|^2$. Let $s = j\omega$, then

$$|H_e(s)|^2 = \frac{\omega^4 / \omega_n^4}{1 + [4\xi^2 - 2]\omega^4 / \omega_n^4 + \omega^4 / \omega_n^4}. \tag{A6}$$

If we choose the damping ratio $\xi = \dfrac{1}{\sqrt{2}} = 0.7071$, then

$$|H_e(s)|^2 = \frac{\omega^4 / \omega_n^4}{1 + \omega^4 / \omega_n^4}. \tag{A7}$$

Third-order Loop

Second, a third-order loop is considered. The second-order filter F(s) is expressed as follows:

$$F(s) = \frac{2\omega_n s^2 + 2\omega_n^2 s + \omega_n^3}{s^2}. \tag{A8}$$

Thus, the overall system is third order, which has three open loop poles at s=0. Hence it is a Type III system. With this Type III system, the steady-state phase error is zero, even if the input is a phase acceleration. Given F(s) in Equation (A8), the resulting closed-loop transfer function is then as expressed follows:

$$H(s) = \frac{\varphi_o}{\varphi_i} = \frac{2\omega_n s^2 + 2\omega_n^2 s + \omega_n^3}{s^3 + 2\omega_n s^2 + 2\omega_n^2 s + \omega_n^3}. \tag{A9}$$

As defined in Equation (A3), the single-sided, closed-loop noise bandwidth (BW) of this third-order loop is [9]

$$BW = \frac{\omega_n}{1.2}. \tag{A10}$$

The phase error to input transfer function ($H_e(s)$) is then defined as:

$$H_e(s) = \frac{\delta\varphi}{\varphi_i} = \frac{s^3}{s^3 + 2\omega_n s^2 + 2\omega_n^2 s + \omega_n^3}. \tag{A11}$$

As we have done for the second-order-loop, we need to calculate the magnitude square of $H_e(s)$. By letting $s = j\omega$, and calculating $|H_e(s)|^2$, we have

$$|H_e(s)|^2 = \frac{\omega^6 / \omega_n^6}{1 + \omega^6 / \omega_n^6}. \tag{A12}$$

Track Loop Errors

The performance of a PLL can be determined by measuring its phase error. The total phase error includes phase jitter and dynamic stress. The 1-sigma value of the phase error is expressed as follows [3]:

$$\sigma_{\delta\varphi} = \sqrt{\sigma_{\delta\varphi w}^2 + \sigma_{\delta\varphi sv}^2 + \sigma_{\delta\varphi rx}^2 + \sigma_{\delta\varphi v}^2} + \frac{\theta_e}{3}, \qquad (A13)$$

where

$\sigma_{\delta\varphi w}$ = 1-sigma phase error due to thermal noise;

$\sigma_{\delta\varphi sv}$ = 1-sigma oscillator phase noise from the satellite's oscillators;

$\sigma_{\delta\varphi rx}$ = 1-sigma oscillator phase noise from the receiver's oscillators;

$\sigma_{\delta\varphi v}$ = 1-sigma vibration induced oscillator jitter;

θ_e = dynamic stress in the PLL tracking loop.

Thermal Noise ($\sigma_{\delta\varphi w}$)

The thermal noise is the most dominant error source of PLL if the system noise bandwidth is in traditional range (10 to 20 Hz). Otherwise, the signal dynamics will cause most of the phase errors. The tracking loop phase error due to thermal noise is given as [3]:

$$\sigma_{\delta\varphi w}^2 = \frac{BW}{C/N0}\left[1 + \frac{1}{2T_{coh}C/N0}\right], \qquad (A14)$$

where BW is the carrier-tracking loop noise bandwidth in Hz; $C/N0$ is the carrier-to-noise ratio; T_{coh} is the coherent integration time. Equation (A14) is obtained when the signal discriminator in Figure 1 is a product detector, I*Q. Equation (A14) holds for a non-coherent carrier tracking loop. The term including T_{coh} in the bracket of (A14) is called squaring loss. It is obvious that a longer T_{coh} and a stronger signal (larger $C/N0$) will mitigate the thermal noise phase error degradation due to squaring loss. If we have perfect knowledge of the carrier phase of the incoming signal, a coherent carrier tracking loop can be implemented. Therefore, the thermal noise phase error, Equation (A15), does not include the squaring loss term [8]. In [11], it is shown that the $\tan^{-1}(Q/I)$ phase discriminator is superior to the I*Q phase discriminator, and approaches the performance of the coherent carrier tracking loop [11].

$$\sigma_{\delta\varphi w}^2 = \frac{BW}{C/N0}. \qquad (A15)$$

In this study the coherent integration time is chosen to be fixed as 1 ms.

Receiver Oscillator Phase Noise ($\sigma_{\delta\varphi rx}$)

The second phase error source is contributed by the receiver oscillator phase noise especially at a low noise bandwidth. One can increase the noise bandwidth such that the PLL can track the clock dynamics. However a higher noise bandwidth introduces more effects on the phase error caused by the thermal noise. To determine an appropriate noise bandwidth, we need to ascertain the carrier phase-noise spectrum. The phase-noise power spectral density (PSD) (one-sided) of oscillator can be written as [12]:

$$G_{rx}(f) = \sum_{k=-4}^{0} h_k f^k, \ f_l \le f \le f_h. \qquad (A16)$$

Outside of the frequency range, the PSD is zero. In this study f_l is set to be zero, while f_h is equal to 500 Hz since the coherent integration time is 1 ms [7]. The coefficients h_k are derived experimentally. The coefficients for TCXO and OCXO used in this study are given by [13] as follows:

h_k	TCXO	OCXO
h_0	5 * 10 ^ -8	5.5 * 10 ^ -8
h_1	6.1905 * 10 ^ -5	5 * 10 ^ -5
h_2	9.6 * 10 ^ -4	6.5 * 10 ^ -4
h_3	0.006	9 * 10 ^ -7
h_4	0.0006	1 * 10 ^ -7

Note that these coefficients are already normalized for the case that the oscillator's center frequency, f_0, is 10.23 MHz.

The 1-sigma oscillator phase noise is then defined as follows [12]:

$$\sigma_{\delta\varphi rx}^2 = \int_0^\infty \left|H_e(s)\right|^2 G_{rx}(f)df. \qquad (A17)$$

Substituting (A16) into (A17), we have

$$\sigma_{\delta\varphi rx}^2 = \int_0^\infty |H_e(s)|^2 \left[\frac{h_4}{f^4} + \frac{h_3}{f^3} + \frac{h_2}{f^2} + \frac{h_1}{f} + h_0 \right] df \quad (A18)$$

Since $f_h = 500$Hz, without losing the accuracy, we can ignore the last two terms in the bracket. So Equation (A18) becomes

$$\sigma_{\delta\varphi rx}^2 = \int_0^\infty |H_e(s)|^2 \left[\frac{h_4}{f^4} + \frac{h_3}{f^3} + \frac{h_2}{f^2} \right] df . \quad (A19)$$

Evaluate (A19) by substituting (A7) and (A12) into (A19) for the second-order and the third-order loops, respectively. Remember that $\omega = 2\pi f$ and change the variables by letting $x = \omega / \omega_n$; apply the following formula:

$$\int_0^\infty \frac{x^{m-1}}{1+x^n} dx = \frac{\pi}{n \sin(\frac{m\pi}{n})}, \quad 0 < m < n .$$

We have 1-sigma oscillator phase noise from the receiver's oscillators for the second-order loop expressed as:

$$\sigma_{\delta\varphi rx}^2 = \frac{(2\pi)^3 h_4}{\omega_n^3} \frac{\pi}{2\sqrt{2}} + \frac{(2\pi)^2 h_3}{\omega_n^2} \frac{\pi}{4} + \frac{(2\pi)h_2}{\omega_n} \frac{\pi}{2\sqrt{2}}$$

in rad^2 and for the third – order loop:

$$\sigma_{\delta\varphi rx}^2 = \frac{(2\pi)^3 h_4}{\omega_n^3} \frac{\pi}{6} + \frac{(2\pi)^2 h_3}{\omega_n^2} \frac{\pi}{3\sqrt{3}} + \frac{(2\pi)h_2}{\omega_n} \frac{\pi}{3}$$

in rad^2.

Finally, if we apply the relationship between BW and ω_n given in (A4) and (A10), we would have $\sigma_{\delta\varphi rx}$ in terms of BW.

Second – order loop ($\xi = \frac{1}{\sqrt{2}} = 0.7071$):

$$\sigma_{\delta\varphi rx}^2 = \frac{(2\pi)^3 h_4}{(1.8856BW)^3} \frac{\pi}{2\sqrt{2}} + \frac{(2\pi)^2 h_3}{(1.8856BW)^2} \frac{\pi}{4}$$
$$+ \frac{(2\pi)h_2}{(1.8856BW)} \frac{\pi}{2\sqrt{2}} \quad (rad \wedge 2) \quad (A20)$$

Third – order loop:

$$\sigma_{\delta\varphi rx}^2 = \frac{(2\pi)^3 h_4}{(1.2BW)^3} \frac{\pi}{6} + \frac{(2\pi)^2 h_3}{(1.2BW)^2} \frac{\pi}{3\sqrt{3}}$$
$$+ \frac{(2\pi)h_2}{(1.2BW)} \frac{\pi}{3} \quad (rad \wedge 2) \quad (A21)$$

Note that the unit BW is Hz. Using (A20) and (A21) to evaluate the variance of phase error due to TCXO and OCXO phase noise for the second-order and the third-order loops, respectively.

Satellite Clock Error

Other than the receiver oscillator on the earth that produces phase noise, the clock onboard in the orbit could also generate phase noise in the signals. From [14], the nominal satellite clock error power spectral density (PSD) can be modeled by the PSD of TCXO; except that the nominal satellite clock error power spectral density (PSD) has to be scaled such that the phase jitter is 0.1 rad when BW is 10 Hz as specified in [15].

Therefore, for the second-order loop, the 1-sigma oscillator phase noise from satellite's oscillators is

$$\sigma_{\delta\varphi sv}^2 = 10\sigma_{\delta\varphi rxTCXO}^2 . \quad (A22)$$

For the third-order loop, the 1-sigma oscillator phase noise from satellite's oscillators is

$$\sigma_{\delta\varphi sv}^2 = 6\sigma_{\delta\varphi rxTCXO}^2 . \quad (A23)$$

Phase Error Due to Vibration

The third phase error is due to the vibration induced oscillator jitter. The PSD of this phase error is given as [7]:

$$G_v(f) = (k_g N f_0)^2 \frac{G_g(f)}{f^2} , \quad (A24)$$

where f_0 is the oscillator's center frequency; N is the ratio between the carrier frequency and the local

oscillator's center frequency; k_g is the oscillator's g-sensitivity in parts/g. In this study, f_0=10.23 MHz and, therefore, $N = f_{L1}/f_0$ =154. A typical value of k_g is 10^{-9} parts/g [14]. Duplicating the plot from [14], we have the PSD of phase error due to vibration $G_v(f)$ as shown in Figure A1.
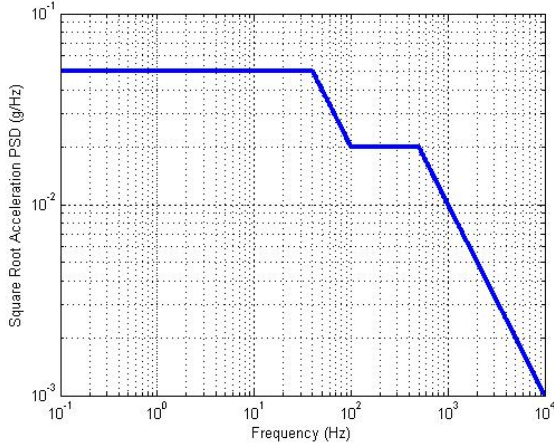

Figure A1: Mechanical Vibration PSD

From Figure A1, we can have the function $G_v(f)$ in following forms:

$G_v(f) = 2.5*10^{-3}$	$f < 40Hz$
$G_v(f) = 2.5*10^{-3}*(\frac{f}{40})^{-2}$	$40 < f < 100Hz$
$G_v(f) = 4*10^{-4}$	$100 < f < 500Hz$
$G_v(f) = 4*10^{-4}*(\frac{f}{500})^{-2}$	$500Hz < f$

Given the PSD $G_v(f)$, we can evaluate the variance of the phase error due to vibration using the following equation:

$$\sigma_{\delta\varphi v}^2 = \int_0^\infty |H_e(s)|^2 G_v(f)df . \qquad (A25)$$

Substituting $|H_e(s)|^2$ for the second-order and the third-order loop as well as the PSD $G_v(f)$ into Equation (A25), we can obtain the values of $\sigma_{\delta\varphi v}^2$ at the various loop noise bandwidths. Note that the above calculation is accomplished by numerical integration since there is no close form for this value.

Dynamic Stress (θ_e)

Due to the abrupt motion, the PLL would experience excessive phase error. Of interest is the peak error, i.e., the phase error transient response of the phase acceleration or phase jerk. For the second-order loop, the phase error due to dynamic stress (phase acceleration) is given by [9]:

$$\theta_e = \frac{\Delta \dot{f}}{\omega_n^2} , \qquad (A26)$$

where Δf is a frequency step in Hz. If $\xi = 0.707$, and from Equation (A4) $\omega_n = \frac{8\xi}{(1+4\xi^2)} BW$, then

$$\theta_e = \frac{\Delta \dot{f}}{(1.885BW)^2} \cong \frac{2.7599 a_{max}}{\lambda_{L1} BW^2} \ in \ cycles,$$

$$\theta_e = \frac{\Delta \dot{f}}{(1.885BW)^2} \cong 2\pi \frac{2.7599 a_{max}}{\lambda_{L1} BW^2} in \ radians , \ (A27)$$

where a_{max} is the maximum value of line-of-sight phase acceleration (g) experienced by the GPS receiver. For a car motion test, we use a value of a_{max} is 0.25g.

Similarly, for the third-order loop the phase error due to dynamic stress (phase jerk) is given by [9]:

$$\theta_e = \frac{\Delta \ddot{f}}{\omega_n^3} \cong \frac{2\pi(5.67) j_{max}}{\lambda_{L1} BW^3} \ in \ radians , \qquad (A28)$$

where j_{max} is the maximum value of line-of-sight jerk experienced by the GPS receiver. A typical value of j_{max} is 0.25g/sec.

So far, we have covered every term for the phase error given in Equation (A13). The following two figures show the plots of Equation (A13) with respect to noise bandwidth. As can be seen in Figures A2 and A3, the unaided third-order PLL has a better phase error performance at a given noise bandwidth than the second-order PLL. These two plots also indicate the fact that thermal noise is dominant in the high bandwidth region while dynamic stress and clock dynamics apparently affect the phase error in the low bandwidth region.
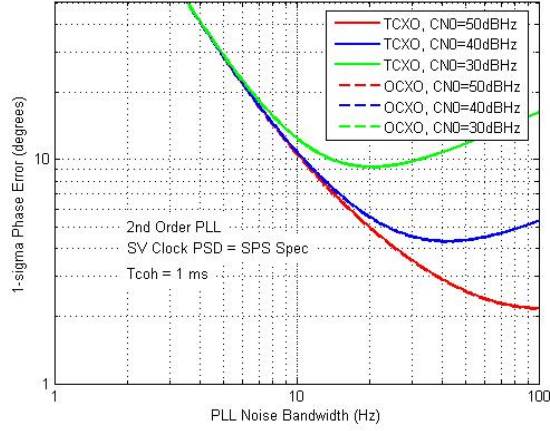
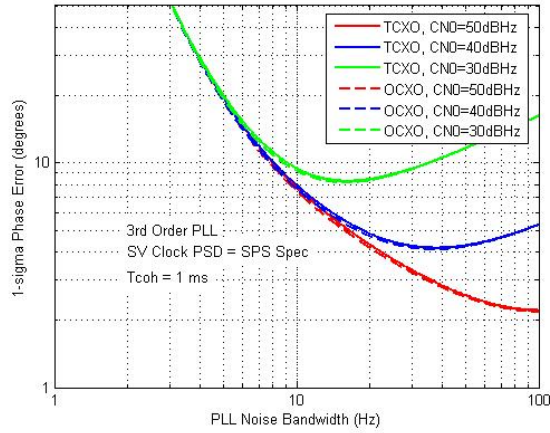**Figure A2: 1-Sigma Phase Error for an Unaided PLL (second-order loop)**

Figure A3: 1-Sigma Phase Error for an Unaided PLL (third-order loop)

Residual Dynamic Stress Error of the Aided PLL

The quantity of interest in this paper is frequency/phase-tracking stability, which can be quantified by the tracking error of the PLL and measured directly by the output of the phase discriminator. We need to quantify the effects of error on the external Doppler estimate. In [7], the upper bound of the 1-sigma Doppler estimate error is 0.1 Hz. We can model this Doppler estimate error as a step in frequency. The effect of this frequency step is evaluated by examining the peak phase error of the tracking loop. Given $\xi = 0.7071$ for the second-order loop, the peak error due to a frequency step input is illustrated in Figure 2.12 of [10] as:

$$\theta_e = 0.45 \frac{\Delta\omega}{\omega_n} = 0.45 \frac{2\pi \, \Delta f}{(1.885 BW)} \, in \ radians \ . \quad \text{(A29)}$$

For the third-order loop, the peak phase error due to a frequency step is equal to the steady-state phase error in a first-order loop described in [9]. Thus, the phase error can be expressed as the following equation:

$$\theta_e = \frac{2\pi \, \Delta f}{4 B_L} \, in \ radians \ . \quad \text{(A30)}$$

Until this step, we have analyzed of phase jitter for both unaided and aided tracking loop. Thus, we have each term of Equation (A13) for both cases. The following Figures show the results of the above model analysis when inertial-aiding is applied. Comparing Figures A4 and A5 with A2 and A3, respectively, we can see the improvement using inertial-aiding PLL.
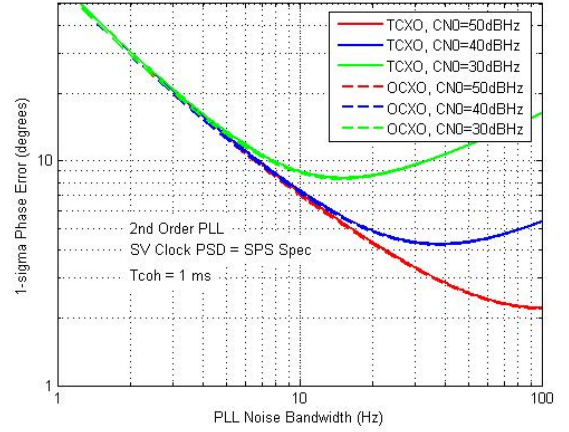

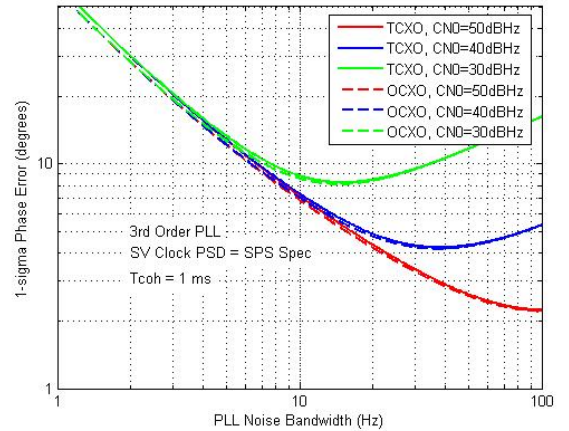**Figure A4: 1-Sigma Phase Error for an Aided PLL (second-order loop)**

Figure A5: 1-Sigma Phase Error for an Aided PLL (third-order loop)

REFERENCES

[1] Johnson, G., Lage, M. and et al, "The JPALS performance Model," Proceeding of the ION-GPS 2003, Portland, OR, September 2003.

[2] Peterson, B. R., Johnson, G. and et al, "Feasible Architectures for Joint Precision Approach and Landing System (JPALS) for Land and Sea," Proceeding of the ION-GPS 2004, Long Beach, CA, September 2004.

[3] Ward, P., Satellite Signal Acquisition and Tracking, in *Understanding GPS Principles and Applications*, Artech House, Washington, D.C., 1996. pp. 119-236.

[4] Bastide, F., Akos, D. and et al, "Automatic Gain Control Control (AGC) as an Interference Assessment Tool," Proceeding of the ION-GPS 2003, Portland, OR, September 2003.

[5] Alban, S., Akos, D. and et al, "Performance Analysis and Architectures for INS-Aided GPS Tracking Loops," Proceedings of ION National Technical Meeting, ION-NTM 2003. Anahiem, CA. January 2003.

[6] Philips, R., and Schmidt, G. T., GPS/INS Integration, AGARD Lecture Series on System Implications and Innovative Application of Satellite Navigation, Paris, France, July 1996.

[7] Gebre-Egziabher, D., Razavi, A., and et al, "Inertial-aided Tracking Loops for SRPS Integrity Monitoring," Proceeding of the ION-GPS 2003, Portland, OR, September 2003.

[8] Misra, P. and Enge, P., *Global Positioning System: Signals, Measurements and Performance*, Ganga-Jamuna Press, Lincoln, Massachusetts, USA, 2001. pp. 356.

[9] Van Dierendonck, A.J., GPS Receivers, in *Global Positioning System: Theory and Applications*, AIAA, Washington D.C., 1996. Vol. 1, pp.329-407.

[10] Best, R. E., *Phase-Locked Loops:Design, Simulations, and Applications*, McGRAW-Hill, Third Edition, 1997. pp1-89.

[11] Gebre-Egziabher, D., and Razavi, A., personal communication entitled "Evaluation of GPS PLL and FLL Architectures in RFI Environments," 2005.

[12] Spilker, J., *Digital Communication by Satellite*, Prentice-Hall, Cambridge, Massachusetts, 1977. pp. 336-397

[13] Alban, S., "Design and Performance of a Robust GPS/INS Attitude System for Automobile Applications", Ph.D. Thesis, Stanford University, 2004

[14] Hegarty, C., "Analytical Derivation of Maximum Tolerable In-band Interference Levels for Aviation Applications of GNSS, journal of The Navigation, Vol. 44, No. 1, 1997. pp. 25-34.

[15] US Department of Defense, *Global Positioning System Standard Positioning Service Signal Specification*, Appendix A, Second Edition, June, 1995.